

THE 4TH INTERNATIONAL CONFERENCE ON ALUMINUM ALLOYS

ON MODELLING THE DEVELOPMENT OF DEFORMATION TEXTURE OF ALUMINIUM

M.J. Young¹, S.K. Choi², P.F. Thomson¹

1. Department of Materials Engineering, Monash University, Clayton, Victoria 3168, Australia

2. CSIRO, Division of Petroleum Resources, P.O. Box 3000, Glen Waverly, Victoria 3150, Australia

Abstract

A Finite Element (FE) model based on rate independent crystal plasticity is presented which can predict the development of deformation textures within FCC materials. Stress equilibrium and strain compatibility are maintained as in real materials. Simulated textures with moderate latent hardening of the slip systems are compared with textures of aluminium alloy 3004 deformed under plane strain compression.

Introduction

A model of polycrystals has been developed as an alternative to models based on the Taylor and Sachs hypotheses in which the microstrain and microstress in each crystal are assumed to be the same as the macrostrain and macrostress of the polycrystalline aggregate respectively. Slip on crystallographic planes and the associated lattice rotation of individual grains in a polycrystalline aggregate are simulated using a 3-dimensional multi-grain Finite Element (FE) model. An explicit time integration scheme is used to solve the governing equations and the evolution of the field and rate equations.

For given constraints on the scale of several hundred grains the model permits inhomogeneous deformation on the grain scale as a result of slip on crystallographic planes within individual elements, as may be observed in real materials. The model ensures that compatibility and equilibrium conditions between grains are always satisfied.

Modelling of the rolling process in which texture and the development of anisotropic properties can be accurately predicted is advantageous. The degree of mechanical anisotropy is a key specification of aluminium sheet quality for demanding manufacturing processes such as deep drawing of 3XXX series alloys for beverage-can body stock.

Yield Surface Based on Interacting Slip Systems

The yield criterion used in the FE model is based on the work by Gambin [1-3]. Gambin [2]

derived a smooth yield condition based on the available slip systems by assuming that they do not act independently. This smooth yield condition may be expressed as:

$$\sum_{r=1}^M \left[\frac{m_i \sigma_{ij} n_j}{k_c^{(r)}} \right]^{2n} = \frac{1}{M} \sum_{s=1}^M \sum_{r=1}^M \left[2 \frac{k_c^{(s)}}{k_c^{(r)}} A_{(ij)}^{(s)} A_{(ij)}^{(r)} \right]^{2n} \quad (1)$$

where:

$$A_{(ij)}^{(r)} = \frac{1}{2} [m_i^{(r)} n_j^{(r)} + m_j^{(r)} n_i^{(r)}] \quad (2)$$

$k_c^{(r)}$ is the critical resolved shear stress for the r -th slip system ($r = 1, 2, 3, \dots, M$), $n_i^{(r)}$ and $m_j^{(r)}$ are the components of the unit vectors normal to the slip plane and along the slip direction respectively, σ_{ij} are the components of the Cauchy stress tensor. For Face Centred Cubic (FCC) materials in which the slip system is $\{111\}[110]$, $M=12$. When $n = 1$ equation (1) reduces to Huber-Mises' yield criterion. As $n \rightarrow \infty$ the approximation to the yield surface tends to that for independent slip. A good approximation to the yield surface based on Schmid's law, with local rounding of corners and vertices is observed when $n = 15$. The smooth yield surface with local rounding ensures uniqueness of plastic deformation while maintaining crystal properties. The plastic strain rate and the plastic spin rate tensors may be expressed by equations (3) and (4) respectively.

$$d_{ij}^p = \lambda \sum_{r=1}^M \frac{1}{2k_c^{(r)}} \left[\frac{m_k^{(r)} \sigma_{kl} n_l^{(r)}}{k_c^{(r)}} \right]^{2n-1} [m_i^{(r)} n_j^{(r)} + m_j^{(r)} n_i^{(r)}] \quad (3)$$

$$\omega_{ij}^p = \lambda \sum_{r=1}^M \frac{1}{2k_c^{(r)}} \left[\frac{m_k^{(r)} \sigma_{kl} n_l^{(r)}}{k_c^{(r)}} \right]^{2n-1} [m_i^{(r)} n_j^{(r)} - m_j^{(r)} n_i^{(r)}] \quad (4)$$

This allows problems to be solved in a manner consistent with the theoretical and numerical framework of plasticity [1].

Technique of Solution

The FE program used here to predict the deformation behaviour and texture development is based on the Dynamic Relaxation (DR) method [4-5]. The governing equations of motion are partially discretised in space using the FE method and solved by a direct explicit time integration using the Central Difference scheme. By satisfying the Courant condition for numerical stability and the adoption of an explicit central difference time integration scheme, computation of strain and constitutive behaviour are decoupled within each time step, allowing direct evaluation of the unknown nodal and other derived field parameters, eliminating the need to set up global stiffness matrices. Besides its effect on numerical stability, the size of the time step is also critical for the accuracy of prediction of texture. One compensation for the small time step is that highly non-linear problems may be solved with only slight additions to the computational requirements.

Equations of Motion: From conservation of linear momentum, the semi-discrete equations of motion for a physically lumped nodal mass M may be expressed as:

$$\frac{\partial v_i}{\partial t} = \frac{F_i}{M} - \alpha v_i \quad (5)$$

$$M \frac{\partial v_i}{\partial t} + F_i^{int} = F_i^{ext} \quad (6)$$

Here v_i is the i -th component of the nodal velocity, F_i^{int} and F_i^{ext} are the i -th components of the internal and external nodal forces respectively, t is time and α is the damping parameter, with:

$$F_i = F_i^{ext} - F_i^{int} \quad (7)$$

The Central Difference scheme was used to solve equation (5) in which the nodal velocity at the mid-time interval during the time increment Δt is given by:

$$v_i^{t+\frac{\Delta t}{2}} = \left[\frac{v_i^{t-\frac{\Delta t}{2}} \left(1 - \frac{\alpha \Delta t}{2}\right) + \frac{F_i^t \Delta t}{M}}{1 + \frac{\alpha \Delta t}{2}} \right] \quad (8)$$

Since constitutive equations were formulated under strain control with a displacement-based spatial discretisation scheme the approach used for analysis of deformation is time step integration of Equation (5). From this integration the velocity gradient field within each element is derived from the computed nodal velocities, the constitutive relation is then invoked to compute all associated incremental quantities over a timestep based on the external and internal variables. This allows the incremental and path dependent nature of plasticity to be modelled.

Large deformation is modelled using an updated Lagrangian scheme. Non-steady state problems are modelled by referring the deformation rate to the last updated configuration.

Discretisation: A piece-wise continuous interpolation (or shape) function was employed to describe the distribution of the spatially discretised unknown nodal parameters $\phi_i^{(t)}$:

$$\phi(x, t) = \phi_I^{(t)} N_I(x) \quad (9)$$

where N_I is the interpolation function with respect to node I . The index I in $\phi_I^{(t)}$ indicates the summation over all nodes of an element. Hence the velocity gradient may be expressed as:

$$\frac{\partial v_i}{\partial x_j} = \frac{\partial N_I}{\partial x_j} v_{iI} \quad (10)$$

and is composed of a symmetric strain rate tensor d_{ij} and an antisymmetric spin rate tensor ω_{ij} which can be written as:

$$d_{ij} = \frac{1}{2} \left(\frac{\partial v_i}{\partial x_j} + \frac{\partial v_j}{\partial x_i} \right) \quad (11)$$

$$\omega_{ij} = \frac{1}{2} \left(\frac{\partial v_i}{\partial x_j} - \frac{\partial v_j}{\partial x_i} \right) \quad (12)$$

The deviatoric and hydrostatic components of the strain rate tensor are computed by selective integration [6]. The total lattice spin, ω_{ij}^L , is calculated as the difference between the total spin and the sum of the elastic and plastic spin tensors:

$$\omega_{ij}^L = \omega_{ij} - (\omega_{ij}^E + \omega_{ij}^P) \quad (13)$$

with the plastic spin calculated from equation (4).

Integration of the Constitutive Equations: Additive decomposition of the total strain tensor into the elastic and plastic parts is assumed, where:

$$\Delta \varepsilon_{ij} = \Delta \varepsilon_{ij}^E + \Delta \varepsilon_{ij}^P \quad (14)$$

$$\dot{\sigma}_{ij} = C_{ijkl} \dot{\varepsilon}_{kl} \quad (15)$$

ε_{ij}^E and ε_{ij}^P are respectively the elastic and plastic parts of the total strain tensor ε_{ij} , σ_{ij} is the Cauchy stress tensor and C_{ijkl} is the elasticity tensor. Correction of the Cauchy stress for rigid body rotation using the antisymmetric part of the velocity gradient, ω_{ij} , is used to get an objective rate of the Zaremba-Jaumann-Noll stress measure $\hat{\sigma}_{ij}$:

$$\hat{\sigma}_{ij} = \dot{\sigma}_{ij} - \omega_{ik} \sigma_{kj} + \sigma_{ik} \omega_{kj} \quad (16)$$

The radial return technique [7] is used for correcting the stress back to the yield surface. The stress correction is applied back towards the origin of the stress deviator space for the yield surface described by equation (1). This is satisfactory when a sufficiently small time step is imposed.

Hardening

An increment in the current critical resolved shear stress $k_c^{(\alpha)}$ is prescribed by the hardening law[2]:

$$k_c^{(\alpha)} = \sum_{\alpha=1}^M h_{\alpha\beta} |\gamma^{(\beta)}| \quad (17)$$

The interaction matrix $h_{\alpha\beta}$ is derived from the type of dislocation interaction between active and non-active slip systems [8]. The interaction components of $h_{\alpha\beta}$ are classified according to the junctions formed between dislocations; dislocations of the same slip system were assigned the coefficient a_0 , those which fail to form junctions, form glissile junctions, or form sessile Lomer-Cottrell locks were assigned coefficients a_1 , a_2 and a_3 respectively. The strength of the dislocation interactions may be equal or increase from a_0 to a_3 .

Simulation of plane strain compression of alloy 3004

Initial simulations of plane strain deformation and texture development have been conducted using meshes constructed from eight-noded brick elements. Each element was initially cubic in shape to represent an equiaxed grain. The mesh represents a small unit of volume of material, in the shape of a rectangular prism, within the plane strain specimen. Each element was randomly assigned orientations from a distribution which represented, statistically, the initial texture of the experimental samples which had a predominantly cube $\{100\}\langle 001 \rangle$ texture. Plane strain boundary conditions were imposed by prescribing compressive displacements on nodes on the top and bottom faces of the mesh; no displacement was allowed on the traverse boundaries. To simulate material in the centre of a plane strain specimen the nodal masses and forces on the short transverse (longitudinal) boundaries were linked to form a periodic boundary. This reproduces the condition of the unit volume situated in the centre of a mesh, allowing it to extend to infinity in the longitudinal directions. The imposition of plane strain boundary conditions did not generally impose plane strain conditions on individual elements in a 3-dimensional mesh. The individual response of each grain to the imposed boundary displacements generated non-uniform reaction forces. The model maintained compatible displacements between adjacent grains.

The mesh used to simulate plane strain compression contained 384 (8x6x8) elements, the orientations and symmetries of which were used to construct pole figures. Simulated pole figures and pole figures measured by X-ray diffraction of the 3004 aluminium samples deformed in plane strain compression were then compared.

Initial simulation of the model was conducted without inclusion of hardening, i.e. $a_0=a_1=a_2=a_3=0$. The predicted textures had strong copper $\{211\}\langle 111 \rangle$ and s $\{123\}\langle 634 \rangle$ components, with the brass $\{110\}\langle 112 \rangle$ component developing rapidly initially then decreasing as grains continued to reorient to the copper or s positions. Deformation within each grain occurred primarily on five or more slip systems in the majority of the 384 grains.

Because aluminium and its alloys are metals of high stacking fault energy, latent hardening was introduced by setting $a_0 = 0$ and $a_1 = a_2 = a_3 > 0$. Texture predicted when low latent hardening were assumed differed little from those predicted when no hardening was assumed. This can be attributed to grains orienting to a position in which five or more slip systems contributed to deformation before any large variations between hardness of slip systems could develop through deformation dominated by less than five slip systems. As the rate of latent hardening was increased, slip became dominant, in the majority of grains, on less than five slip systems. This increased the brass $\{110\}\langle 112 \rangle$ component. The integrated densities (volume fractions) of five major components of recrystallization and rolling texture developed in plane strain compression samples of 3004 alloy at 22, 33 and 40% strain and the corresponding simulated deformation textures are shown in Table I. Latent hardening was introduced such that the critical shear stress on latent systems became significantly different from that on the active systems, (which generally numbered less than five). Figures 1(a), (b) and (c) show the pole figures ((111), (200) and (220)) for the plane strain compression of 3004 alloy at 22, 33 and 40% strain; Figure 1(d), (e) and (f) show the corresponding predicted textures.

Table I. Percentage volume fractions of five major texture components in observed and simulated samples at 22, 33 and 40% strain*

Component	Name	22% Strain		33% Strain		40% Strain	
		Exp.	Theor.	Exp.	Theor.	Exp.	Theor.
$\{110\}\langle 112 \rangle$	brass	25	33	27	22	31	25
$\{211\}\langle 111 \rangle$	copper	10	16	28	30	21	37
$\{123\}\langle 634 \rangle$	s	11	12	17	18	21	19
$\{100\}\langle 001 \rangle$	cube	18	7	11	4	8	4
$\{110\}\langle 001 \rangle$	goss	28	12	23	13	15	12

* The difference between 100% and sum of the five texture components can be attributed to the random component.

Discussion

Textures simulated by the FE model show good agreement with those observed aluminium alloy 3004 developed in plane strain deformation. The introduction of latent hardening to the model shows that a copper to brass transition may be obtained. This may be attributed to a reduction in the number of active slip system and behaviour similar to that predicted by models of the Sachs type [9], but unlike the Sachs model, compatibility of strain is maintained between grains.

The model has several advantages over models of deformation texture of the Taylor, Sachs or self-consistent[10] type. The model admits grain-to-grain interactions and is capable of incorporating different types of elements to model inhomogeneity at the grain scale and to investigate their effect on the overall development of texture. Grain boundaries may be modelled using interface elements.

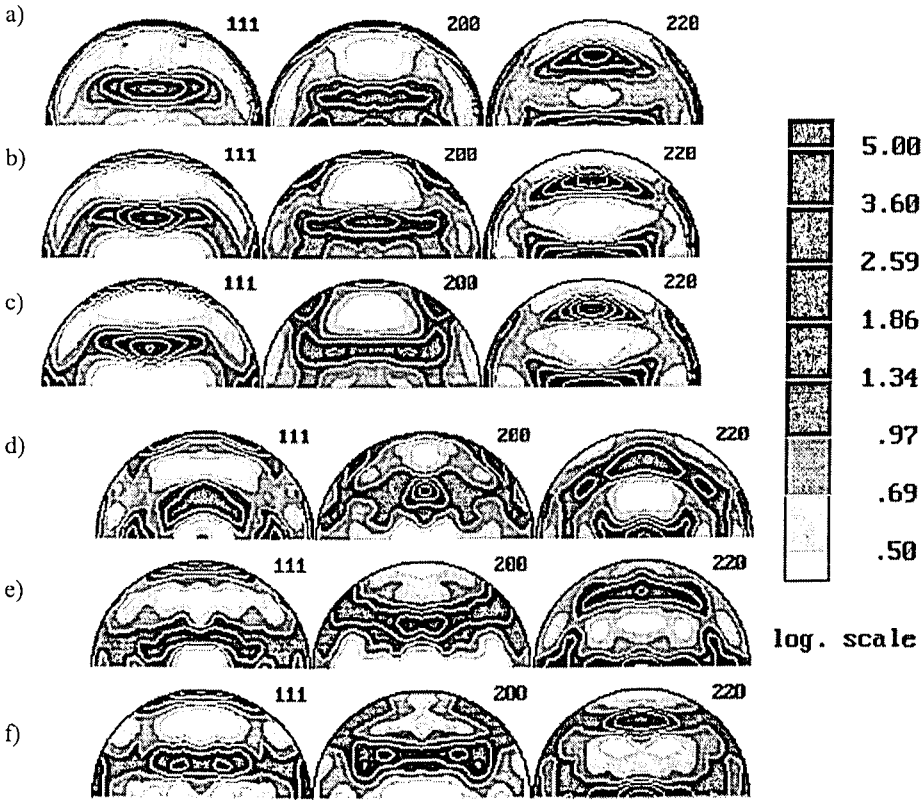


Figure 1. Plane strain deformation textures. Experimental at (a)22%, (b)33% and (c)40% strain and simulated at (d) 22%, (e)33% and (f)40% strain.

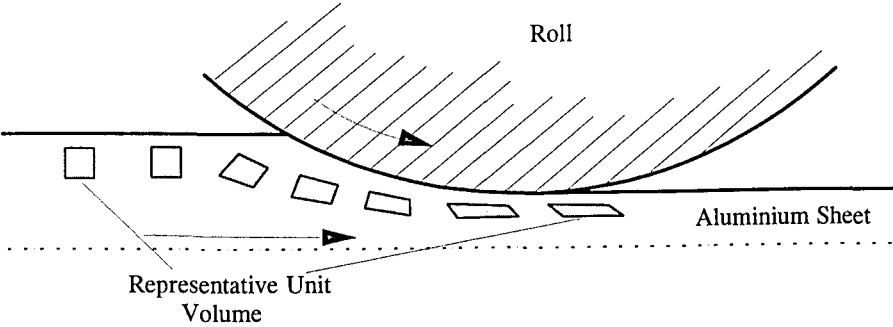


Figure 2. Schematic diagram of the strain path of a representative unit volume as it passes through the roll gap.

The model is intended for determining the texture variations which occur during the rolling of aluminium. It is intended that a mesh similar to that used to simulate plane strain deformation will be subjected to the deformation history of a representative unit volume of material passing through the roll gap, determined from an existing FE model of rolling, as illustrated in Figure 2. This will permit simulation of rolling textures and the investigation of deformation texture as a function of position in the roll gap, reduction and friction.

Conclusion

A Finite Element model based on crystal plasticity has been described which maintains strain compatibility and stress equilibrium in a polycrystalline aggregate. Results from the model compare favourably with textures observed in 3004 aluminium alloy subjected to deformation in plane strain. When no hardening is assumed the model predicts a strong copper $\{211\}\langle 111 \rangle$ texture component and five slip systems are observed to dominate slip in most grains. As the assumed rate of latent hardening is increased the brass component of texture $\{110\}\langle 112 \rangle$ increases in intensity and less than five of the active slips systems were observed to dominate slip in most grains and texture tends towards that predicted by models of the Sachs type[9]. It is intended that the model will be further developed and applied to the prediction of the effects of rolling parameters on rolling textures developed.

References

1. W. Gambin, Z. angew. Math. Mech. **71**, (1991), T265.
2. W. Gambin, Int. J. Solids Structures **29**, (1992), 2013.
3. W. Gambin, Modelling of plastic deformation and its engineering applications, ed. S.I. Andersen et al. (Risø National Laboratory, Roskilde, Denmark: 13th Int. Symp., 1992), 271-276.
4. A.S. Day, The Engineer **219**, (1965), 218.
5. J.R.H. Otter, Proc. Int. Civ. Engrs. **35**, (1966), 633.
6. D.S. Malkus and T.J.R. Hughes, Comp. Meth. Appl. Mech. Eng. **15**, (1978), 63.
7. R.D. Krieg and B.D. Krieg, J. Press. Vess. Technol. **99**, (1977), 510.
8. P. Franciosi and A. Zaoui, Acta Metall. **30**, (1982), 1627.
9. T. Leffers (1979), Strength of Metals and Alloys, Vol. 2 ed. P. Hansen et al. (Aachen, 27-31 Aug, 1979), 769.
10. A. Morawiec et al., Phil. mag A. **64**, (1991), 1251.

Acknowledgment

This work is currently funded under an Australian Postgraduate Research Award, Industrial sponsor- Comalco Research and Technology